

---

---

PARTICLE ACCELERATION  
IN PLASMA

---

---

## 2.5-Dimensional Numerical Simulation of a High-Current Ion Linear Induction Accelerator

O. V. Bogdan, V. I. Karas', E. A. Kornilov, and O. V. Manuilenko

*National Science Center Kharkiv Institute of Physics and Technology, vul. Akademichna 1, Kharkiv, 61108 Ukraine*

Received February 11, 2008

**Abstract**—Results are presented from numerical particle simulations of the transport and acceleration of a high-current tubular ion beam through one to five magnetically insulated accelerating gaps. The ion beam is neutralized by an accompanying electron beam. The possibility of transporting a high-current neutralized ion beam through five cusps is demonstrated. It is shown that the quality of the distribution function of a high-current ion beam at the exit from the accelerator can be substantially improved by optimizing the energy of the neutralizing electron beam. It is also shown that, by injecting additional high-current electron beams into the cusps, the accelerated ion beam can be made more monoenergetic and its divergence can be reduced.

PACS numbers: 41.75.-i, 52.40.Mj, 52.58.Hm, 52.59.-f, 52.65.Rr

DOI: 10.1134/S1063780X08080059

### 1. INTRODUCTION

Two methods for producing high-current ion beams (HCIBs) by linear accelerators—linacs—are now being considered for applications in inertial confinement fusion (ICF) [1–3]. The first method is based on linear resonance accelerators with storage rings, and the second, on induction linacs. The advantages of the first method are high acceleration rate (1–5 MeV/m) and high efficiency (up to 30%). The final ion energy should be as high as 100 GeV. The accelerated ions are accumulated in storage rings and are then passed into compression rings, which shorten the pulse duration. The pulse should be compressed in time by a factor of more than  $10^4$ .

The method based on a vacuum induction linac (LIA) [1, 2, 4–7] implies the simultaneous acceleration of 16 to 120 (depending on the particular scheme) ion beams in quadrupole lenses, where they are focused in the transverse direction. During the acceleration, the number of ion beams becomes smaller because some of them are merged into one. The final ion energy should be on the order of 10 GeV with an energy content on the order of 10 MJ, the pulse duration being several tens of nanoseconds. The advantages of this approach are that the LIA can operate at a high repetition rate, can accelerate high-current beams of ions of almost any species with a high efficiency (more than 30%; see, e.g., [7]), and provides a simple and natural way to shorten the current pulse duration during the acceleration process (so there is no need for additional operations to amplify the current pulse by compressing it in time). Another approach to using an LIA to generate HCIBs from ions with velocities much lower than the speed of light is to utilize not vacuum systems for transporting beams—quadrupoles and solenoids—but collective focusing

techniques in which the space-charge forces of an ion beam are neutralized by electrons [2, 8–13] and the electron current is suppressed by the magnetic insulation of the accelerating gaps [14]. In such an LIA with charge- and current-neutralized HCIBs in a magnetically insulated accelerating gap, the ion current during acceleration can be as high as tens of kA. For ICF purposes, this means that the final ion energy can be lowered to several hundreds of MeV, while keeping the required energy content of the beams on the target unchanged [2]. In addition, there is no need for storage complexes on multistage compression of the ion current pulses.

Since the linacs under consideration are axisymmetric, the well-known mechanism for transporting a charge- and current-neutralized ion beam (NIB) through a magnetic barrier [15] does not operate because the azimuthal polarization electric field cannot arise.

The mechanism for charge and current neutralization of an HCIB by an electron beam in an axisymmetric accelerating gap was proposed and investigated in [14, 16–18], in which a study was made of the electron and ion dynamics in a cusp magnetic field geometry in the presence of a constant accelerating electric field in the single-particle approximation and also of the effect of the electric and magnetic self-fields of the electron and ion beams on their passage through a cusp and on the magnetic insulation. The physical meaning of the mechanism for charge and current neutralization of a tubular HCIB in a magnetically insulated accelerating gap is as follows: the neutralization is provided by a specially injected electron beam, which drifts through the cusp in a self-consistent azimuthal magnetic field and a self-consistent electric field that arises from

a slight radial separation between the ion and electron beams.

Let us briefly outline the conditions for transporting and accelerating an HCIB through an axisymmetric system with magnetic insulation. The external magnetic field has a cusp axisymmetric configuration,

$$\begin{aligned} H_r &= -H_0 I_1(kr) \sin(kz), \\ H_z &= -H_0 I_0(kr) \cos(kz), \end{aligned} \quad (1)$$

where  $r$  is the transverse coordinate,  $z \in [0, L]$  is the longitudinal coordinate,  $L$  is the cusp length,  $k = \pi/L$ ,  $H_0$  is the external magnetic field, and  $I_0(x)$  and  $I_1(x)$  are modified Bessel functions. Let a tubular electron beam and tubular ion beam of the same cross section and the same current density  $|q_e|n_e V_e = q_i n_i V_i$  (where  $q$  is the charge of a particle,  $n$  and  $V$  are the particle density and velocity, and the subscripts  $e$  and  $i$  stand for electrons and ions) be injected into a system with cusp external magnetic field (1) and a longitudinal accelerating electric field  $E_z$ . In order for an electron beam to drift through the gap for ion acceleration and, accordingly, to neutralize the charge and current of an HCIB, the electron energy  $\epsilon_{0e}$  should be low enough that the electron gyroradius is less than the characteristic cusp length  $L$  (the drift condition), on the one hand, and, on the other, it also should be higher than the energy lost by the electrons in passing through the gap (the condition for the ion beam not to be “loaded” with the electron beam):

$$|q_e| E_z L < \epsilon_{0e} \ll \frac{q_e^2 H_0^2 I_0^2(ka) L^2}{2m_e c^2}. \quad (2a)$$

Here,  $m_e$  is the mass of an electron,  $c$  is the speed of light, and  $a$  is the beam radius.

In cusp geometry, the presence of a longitudinal electric field gives rise to azimuthal electron drift with the velocity  $V_{ed\phi}$ . The drift in turn changes the  $H_r$  and  $H_z$  components of the magnetic field (1) in the system: the longitudinal motion of charged particles excites the azimuthal magnetic field  $\tilde{H}_\phi$ . Since their gyroradius is small, the injected electrons moving along the magnetic surfaces determined by the injection conditions tend to go away from the ions moving along straight trajectories. The resulting slight radial separation between the electron and ion beams produces the radial electric field  $\tilde{E}_r$ . In the radial electric and azimuthal magnetic fields, the electrons drift in the longitudinal direction. The electron drift velocity  $V_{edz}$  is quadratic in the ion beam density (since  $\tilde{E}_r$  and  $\tilde{H}_\phi$  are proportional to  $n_i$ ). This velocity will be close to the velocity  $V_i$  of the HCIB—a condition that provides not only the current neutralization of the ion beam but also its charge neutralization because the electron and ion currents are the

same—only when the current of the injected electron beam is sufficiently high. It should be noted that a system utilizing electron and ion beams such that the electron and ion currents are the same and the drift velocity of the electron beam is close to the ion velocity has an additional advantage—it ensures that the efficiency of the induction section creating the accelerating electric field is high throughout the entire pulse: under these conditions, the section operates in an idle mode because the total current is nearly zero. The external magnetic and accelerating electric fields satisfy the equations  $\nabla \cdot \mathbf{H} = 0$ ,  $\nabla \times \mathbf{H} = 0$ , and  $\nabla \cdot \mathbf{E} = 0$ ; consequently, for the self-consistent magnetic and self-consistent radial electric fields, we obtain the following set of equations:

$$\begin{aligned} \frac{1}{r} \frac{\partial}{\partial r} (r \tilde{H}_r) + \frac{\partial \tilde{H}_z}{\partial z} &= 0, \quad V_{ed\phi} = c \frac{E_z H_r}{H^2}, \\ \frac{\partial}{\partial r} \left( \frac{1}{r} \frac{\partial}{\partial r} (r \tilde{H}_r) \right) + \frac{\partial^2 \tilde{H}_r}{\partial z^2} &= \frac{4\pi q_e}{c} \frac{\partial}{\partial z} (n_e V_{ed\phi}), \\ \frac{1}{r} \frac{\partial}{\partial r} (r \tilde{H}_\phi) &= \frac{4\pi}{c} \left( q_i n_i V_i + q_e \bar{n}_e c \frac{\tilde{E}_r \tilde{H}_\phi}{H^2} \right), \\ \frac{1}{r} \frac{\partial}{\partial r} (r \tilde{E}_r) + \frac{\partial \tilde{E}_z}{\partial z} &= 4\pi (q_i n_i + q_e \bar{n}_e), \end{aligned}$$

$$\bar{n}_e = n_i \frac{q_i}{|q_e|} \frac{V_i H^2}{c \tilde{E}_r \tilde{H}_\phi}.$$

Usually, a tubular beam has a thin wall ( $\Delta \ll a$ ) and its radius is small in comparison with the cusp length ( $a \ll L$ ). From the second equation in the set, we can find that the magnetic field excited by the azimuthal electron drift is much weaker than the external cusp magnetic field when the initial density of the electron beam satisfies the inequality

$$n_e \leq \frac{H_0^2 I_1^2(ka)}{4\pi |q_e| E_z L} \left( \frac{L}{a} \right)^2. \quad (2b)$$

From Poisson’s equation we can see that, when the longitudinal drift velocity of the electron beam,  $V_{edz}$ , is close to the ion velocity  $V_i$ , the charge of an HCIB is neutralized essentially completely and the self-consistent longitudinal electric field  $\tilde{E}_z$  is weak. In this case, the radial electric field  $\tilde{E}_r$  is estimated by

$$\tilde{E}_r \approx 4\pi q_i n_i \delta, \quad \delta_{\min} < \delta < \delta_{\max} \leq \Delta,$$

where  $\delta_{\max} = (q_i \epsilon_{0e} / |q_e| m_i \omega_{pi}^2)^{1/2}$  and  $\delta_{\min} = (q_i (\epsilon_{0e} - |q_e| E_z L) / |q_e| m_i \omega_{pi}^2)^{1/2}$ .

The equation for the magnetic field  $\tilde{H}_\phi$  yields the following estimate for its maximum strength near the radius  $a$ :

$$\tilde{H}_\phi \approx 4\pi q_i n_i \frac{V_i}{c} \delta.$$

In order for the drift velocity of the electron beam to be close to the ion beam velocity  $V_i$  within the entire accelerating gap, the density of the ion beam and its thickness should satisfy the inequalities

$$n_i \geq \frac{H_0^2 I_1^2 (ka)}{4\pi(\epsilon_{0e} - |q_e| E_z L)}, \quad \Delta \geq \frac{c\Omega_i}{\omega_i^2}, \quad (3)$$

where  $\Omega_i = q_i H / (m_i c)$  and  $\omega_i = \sqrt{4\pi q_i^2 n_i / m_i}$  are the ion gyrofrequency and ion Langmuir frequency, respectively. The first of conditions (3) implies that the current of the transported ion beam should be sufficiently high. The second of the conditions shows how strong the self-consistent fields should be. That a high-current NIB can be transported and accelerated under the above conditions was demonstrated numerically in [16–18].

In the present paper, we report the results of numerical particle simulations of the transport and acceleration of a tubular HCIB through several magnetically insulated accelerating gaps. The ion beam is neutralized by an accompanying electron beam. The simulations involve solving a complete set of Maxwell's equations. We show that a high-current NIB can be transported through one to five cusps. We find that, when conditions (2) and (3) fail to hold, the neutralizing electron beam is lost, so an HCIB cannot be transported. We determine how the quality of the distribution function of an HCIB at the exit from the accelerator is related to the energy of the accompanying electron beam. We also analyze how the injection of additional high-current electron beams into the cusps affects the energy spread of the ions in the accelerated beam and the beam divergence at the exit from the accelerator.

## 2. MATHEMATICAL MODEL

The self-consistent dynamics of beam–plasma systems in external electromagnetic fields is described by relativistic Vlasov equations or (when collisions are important) Boltzmann equations for the distribution functions of electrons, ions, and (if necessary) neutrals and also by Maxwell's equations. Numerical particle simulations are based on repeating the computational procedure of (a) integrating the Vlasov equations along the characteristics,

$$\frac{d\mathbf{p}}{dt} = q_s \mathbf{E} + \frac{q_s}{c} \mathbf{v} \times \mathbf{B}, \quad \frac{d\mathbf{r}}{dt} = \mathbf{v}, \quad \mathbf{p} = m_s \mathbf{v} \gamma, \quad (4)$$

where the electric and magnetic fields  $\mathbf{E} = \mathbf{E} + \mathbf{E}_{\text{ext}}$  and  $\mathbf{B} = \mathbf{B} + \mathbf{B}_{\text{ext}}$  are a superposition of the given and self-

consistent fields,  $\mathbf{r}$  is the position vector of a particle, and  $\mathbf{p}$  and  $\mathbf{v}$  are its momentum and velocity; (b) calculating the charge and current densities,  $\rho(\mathbf{r}, t)$  and  $\mathbf{j}(\mathbf{r}, t)$ ,

$$\rho(\mathbf{r}, t) = \sum_s q_s \int f_s(\mathbf{p}, \mathbf{r}, t) d\mathbf{p},$$

$$\mathbf{j}(\mathbf{r}, t) = \sum_s q_s \int \mathbf{v} f_s(\mathbf{p}, \mathbf{r}, t) d\mathbf{p},$$

where  $f_s(\mathbf{p}, \mathbf{r}, t)$  is the distribution function of the particles of species  $s$ ; and (c) solving Maxwell's equations

$$\frac{1}{c} \frac{\partial \tilde{\mathbf{E}}}{\partial t} = \nabla \times \mathbf{H} - \frac{4\pi}{c} \mathbf{j}(\mathbf{r}, t), \quad \frac{1}{c} \frac{\partial \mathbf{B}}{\partial t} = -\nabla \times \mathbf{E}, \quad (5)$$

$$\nabla \cdot \mathbf{E} = 4\pi \rho(\mathbf{r}, t), \quad \nabla \cdot \mathbf{B} = 0. \quad (6)$$

A computational cycle in the particle simulation method consists in the following. The positions of the particles are calculated at discrete times  $t^n$  in a continuous space of coordinates and velocities,

$\left\{ \mathbf{v}_i \left( t^{n+\frac{1}{2}} \right), \mathbf{r}_i(t^n) \right\}$ , and the fields are calculated at discrete points on a spatial mesh at discrete times,

$\left\{ \mathbf{E}_j(\mathbf{r}_j, t^n), \mathbf{B}_j \left( \mathbf{r}_j, t^{n+\frac{1}{2}} \right) \right\}$ . The positions of macroparticles in the phase space  $\{ \mathbf{v}_i, \mathbf{r}_i \}$  at the initial time  $t = 0$

are specified. At each time step  $\Delta t$ , the charge and current densities on the mesh are calculated from the known macroparticle distribution with the help of a certain weighting technique,  $\{ \mathbf{v}_i, \mathbf{r}_i \} \rightarrow \{ \rho_j, \mathbf{j}_j \}$ . Maxwell's equations are solved in order to determine the field distributions  $\{ \mathbf{E}_j, \mathbf{B}_j \}$  on the mesh from the charge and current densities  $\{ \rho_j, \mathbf{j}_j \}$  calculated at the preceding time step of the computational procedure,  $\{ \rho_j, \mathbf{j}_j \} \rightarrow \{ \mathbf{E}_j, \mathbf{B}_j \}$ . The forces acting on each macroparticle are calculated by applying the corresponding weighting technique,  $\{ \mathbf{E}_j, \mathbf{B}_j \} \rightarrow \mathbf{F}_i$ . The equations of motion are integrated and the new velocities and coordinates of the macroparticles are determined,  $\mathbf{F}_i \rightarrow \{ \mathbf{v}'_i, \mathbf{r}_i \}$ . It is checked whether the macroparticles cross the boundaries of the computation region. If they do, then they are either excluded from computations or introduced in the corresponding scenario of the interaction with the wall as (a) particles reentered into the computation region, e.g., according to the elastic reflection laws, or as (b) injected secondary particles. This time step of the numerical procedure also models the injection of beam particles into the computation region. And finally, if necessary, a Monte Carlo scenario is sampled that involves collisions among the particles and their collisions with neutrals as well as their appearance, disap-

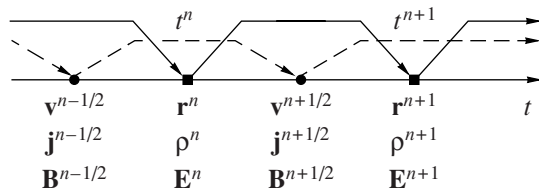


**Fig. 1.** Schematic of the leap-frog (alternative-direction) integration method. The charge densities  $\rho$ , electric fields  $\mathbf{E}$ , and electrostatic potentials  $\Phi$  are calculated on the same time layers  $t^n$  as the particle coordinates  $\mathbf{r}$ . The current densities  $\mathbf{j}$  and magnetic fields  $\mathbf{B}$  are calculated on the same time layers  $t^{n+\frac{1}{2}}$  as the particle velocities  $\mathbf{v}$ .

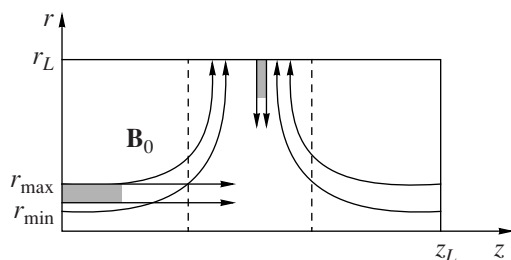


**Fig. 2.** Configuration of the lines of the external magnetic field and regions of injection of a tubular electron beam and tubular ion beam, as well as an additional electron beam, into the computation region.

pearance, and scattering [19–23]. The computational cycle—one time step—is thus completed.

The particles and fields are sequentially shifted in time as is shown in Fig. 1. The positions of the particles and their velocities are shifted in time by half a time step. This shift is motivated by the method chosen for discretizing equations of motion (4)—a leap-frog centered explicit difference scheme of second-order accuracy. The integration over time is carried out by using the Boris scheme [24], which is stable for  $\omega_0 \Delta t < 2$ , where  $\omega_0$  is the characteristic frequency of the problem. In our simulations, we had  $\omega_0 \Delta t \ll 1$ .

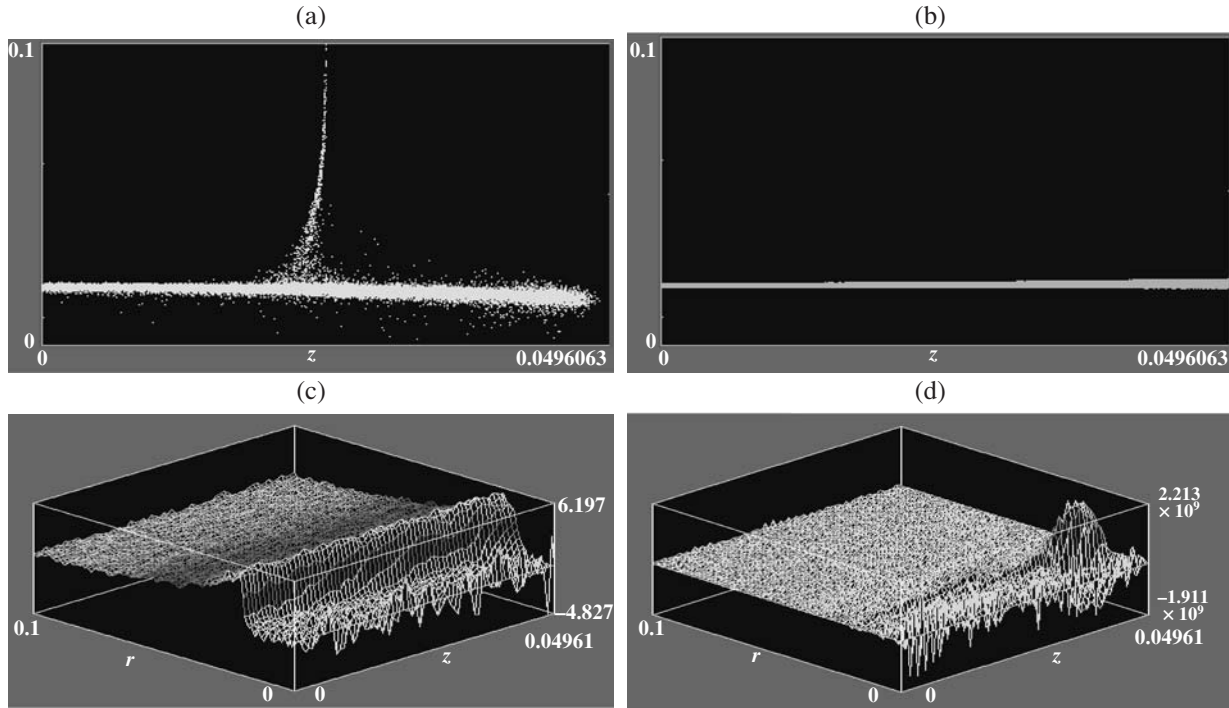
Maxwell's equations (5) are discretized in space and time and are solved by a leap-frog explicit finite-difference scheme [25]. The fields  $\mathbf{E}$  are calculated at the centers of the boundaries of the computational cells at the times  $t = n\Delta t$ , and the magnetic fields are calculated at the centers of the faces of the cells at the times  $t = (n + 1/2)\Delta t$ . The scheme is of second-order accuracy in space and time. It is stable for uniform meshes provided that the Courant–Levi condition is satisfied:  $\Delta t \leq$

$\frac{1}{c} \left( \sum_m \frac{1}{(\Delta x_m)^2} \right)^{-\frac{1}{2}}$ , where  $\Delta x_m$  is the spatial step, with  $m$  being the coordinate index. The scheme for solving

Eqs. (5) numerically does not generally ensure that the charge is continuous. The reason is that, in our particle-in-cell (PIC) simulations, the charge and current densities are calculated independently, using a bilinear weighting. This is why, in earlier papers [16–18], the potential component of the electric field was corrected by the Boris method (see, e.g., [24]). This approach requires that Poisson's equation be solved within the entire computation region. A more effective technique for correcting the potential component of the electric field—the one that does not involve solving Poisson's equation—is the Langdon–Marder method [26]. Mardahl and Verboncoeur [27] showed that both of the methods give essentially the same accuracy. An effective tool for increasing the computational speed is also provided by charge-conserving schemes for calculating the current density on a mesh [28–30]. The algorithms described above—in particular, those for solving the equations of motion and Maxwell's equations and for correcting the potential component of the electric field on the basis of Langdon–Marder method, as well as the charge-conserving scheme for calculating the current density on a mesh—were implemented into the easily modifiable and extendable object-oriented PIC code XOOPIC [30]. The results of numerical experiments reported below were obtained by using the charge-conserving scheme for calculating the current density on a mesh [30]. As for computations in which the potential component of the electric field was corrected based on the Langdon–Marder method, they were carried out for several versions of the input parameters and their results were used as test ones.

### 3. SIMULATION RESULTS

Figure 2 shows the axial cross section of the single-cusp accelerating structure under simulation, external magnetic field configuration (1), and the regions where the beams are injected. The length of the system is  $z_L = 0.05$  m and its radius is  $r_L = 0.1$  m. The first one-third of the system is the drift space, the second one-third is the accelerating gap (in the second half of which an additional electron beam can be injected), and the third one-third is the drift space. A tubular magnetized electron beam and tubular unmagnetized ion beam are continuously injected into the system from the left. The minimum radii of the electron and ion beams are the same, as well as their maximum radii,  $r_{\min} = 0.0189$  m and  $r_{\max} = 0.0205$  m, the current densities at the time of injection being equal to one another. The multicusp systems to be simulated are formed by connecting additional cusps from the right. The outer boundaries of the system are perfectly conducting metal walls. The particles that come into contact with the metal boundaries are excluded from computations. Hereafter, linear dimensions are in m, magnetic fields are in units of 10 kG, electric fields are in V/m, and particle energies are in eV.



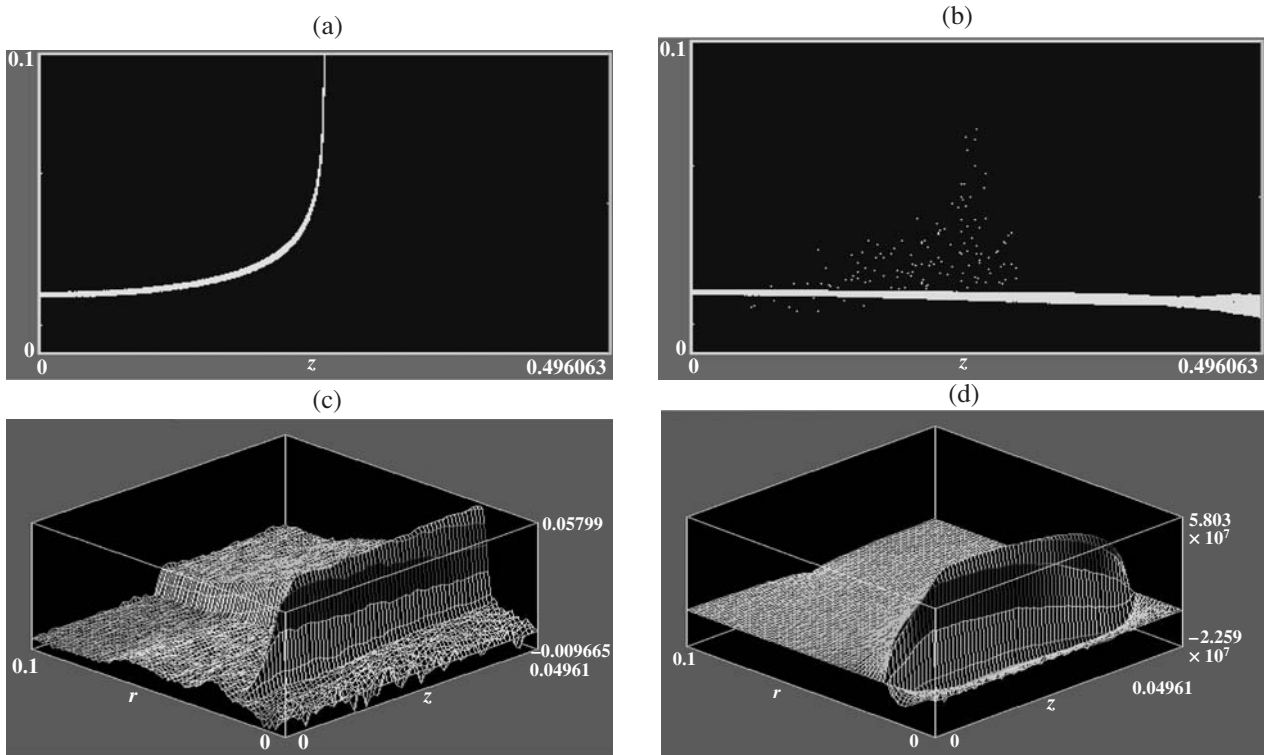
**Fig. 3.** Transport of a high-current NIB through a single cusp: (a) electron and (b) ion distributions in the  $\{r, z\}$  plane (with  $r$  and  $z$  being the transverse and longitudinal coordinates, respectively); (c) azimuthal component of the self-consistent magnetic field,  $B_\phi(r, z)$ ; and (d) radial component of the self-consistent electric field,  $E_r(r, z)$ . The parameters are  $H_0 = 47$  kG,  $v_{e0} = 0.85c$ ,  $v_{i0} = 0.21c$ , and  $n_{e0} = 7 \times 10^{19} \text{ m}^{-3}$ .

Figure 3 illustrates the results of numerical simulations of the transport ( $E_z = 0$ ) of a high-current tubular NIB through a single cusp under conditions (2) and (3). Figures 3a and 3b show the electron and ion distributions in the  $\{r, z\}$  plane. Figures 3c and 3d show the fields in which the electrons accompanying the ion beam drift, specifically, the azimuthal component of the self-consistent magnetic field,  $B_\phi(r, z)$ , and the radial component of the self-consistent electric field,  $E_r(r, z)$ . From Fig. 3a we can see that most of the electrons accompanying the ion beam penetrate into the second half of the cusp. But at the center of the cusp, some beam electrons are lost, so the space charge of the ion beam in the second half of the cusp is slightly unneutralized and the ion beam becomes wider there (Fig. 3b). For comparison, Fig. 4 presents the results of simulating the transport of a low-current NIB through a single cusp when conditions (2) and/or (3) fail to hold. In this case, the self-consistent field components  $B_\phi$  and  $E_r$  are far weaker than those in the previous case and the electrons cannot drift into the second half of the cusp, with the result that the electron beam is lost and the ion beam in the second half becomes wider.

Transport conditions (2) and (3) can be violated when the radii of the beams injected into the cusp are changed. Figure 5 illustrates the results of simulating the transport of a high-current tubular NIB through

three cusps. The physical parameters of the problem are the same as those in Fig. 3, except for the number of cusps (three versus one) and the beam injection radii: in Figs. 5a and 5b, the radii  $r_{\min}$  and  $r_{\max}$  are decreased by  $0.25r_{\min}$  (conditions (2) and (3) are satisfied) and, in Figs. 5c and 5d, these radii  $r_{\min}$  and  $r_{\max}$  are increased by  $r_{\min}$  (conditions (2) and/or (3) are violated). Figures 5a and 5b show a situation similar to that with transport through a single cusp: as high-current ion and electron beams are transported simultaneously through three cusps, some of the beam electrons are lost at the center of each cusp, so the space charge of the ion beam becomes unneutralized and the ion beam becomes wider. When conditions (2) and/or (3) fail to hold, the transport is impossible (see Figs. 5c, 5d).

Figures 6a, 6c, and 6e illustrate the results of simulating the transport of a high-current NIB through four cusps, and Figs. 6b, 6d, and 6f demonstrate the results of simulating the transport through five cusps. The physical parameters of the problem are the same as those in Fig. 3. From Figs. 6e and 6f, which show the ion distribution functions  $F_i(\epsilon, r)$  over energy and over the transverse coordinate at the right boundaries of the (e) fourth and (f) fifth cusps, we can see that the main group of the ions escaping from the last (fifth) cusp is concentrated around the beam injection radius. An analysis of the distribution functions  $F_i(\epsilon, r)$  for the



**Fig. 4.** Transport of a low-current NIB through a single cusp: (a) electron and (b) ion distributions in the  $\{r, z\}$  plane; (c) azimuthal component of the self-consistent magnetic field,  $B_\phi(r, z)$ ; and (d) radial component of the self-consistent electric field,  $E_r(r, z)$ . The parameters are  $H_0 = 47$  kG,  $v_{e0} = 0.85c$ ,  $v_{i0} = 0.21c$ , and  $n_{e0} = 7 \times 10^{17} \text{ m}^{-3}$ .

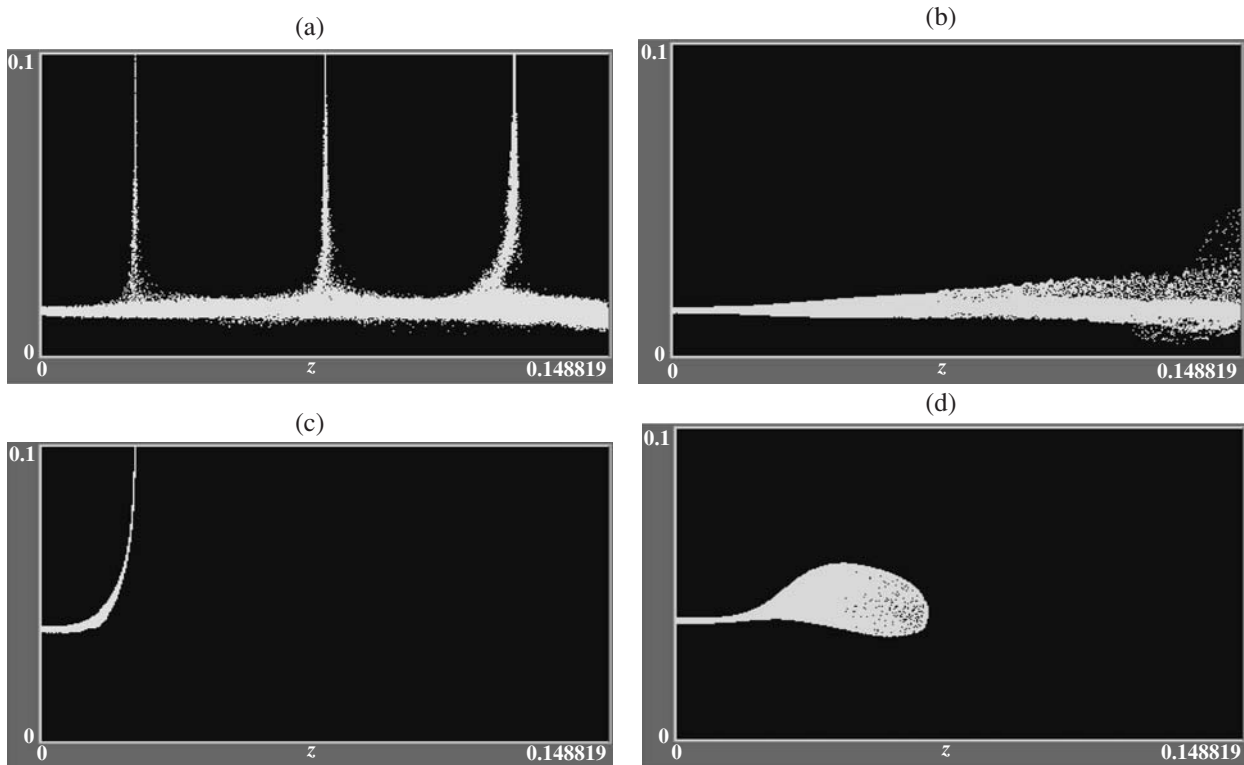


**Fig. 5.** Transport of a high-current NIB through three cusps: (a, c) electron and (b, d) ion distributions in the  $\{r, z\}$  plane for the beam radii (a, b)  $r_{\min} = 0.0142$  m and  $r_{\max} = 0.0158$  m and (c, d)  $r_{\min} = 0.0378$  m and  $r_{\max} = 0.0394$  m.

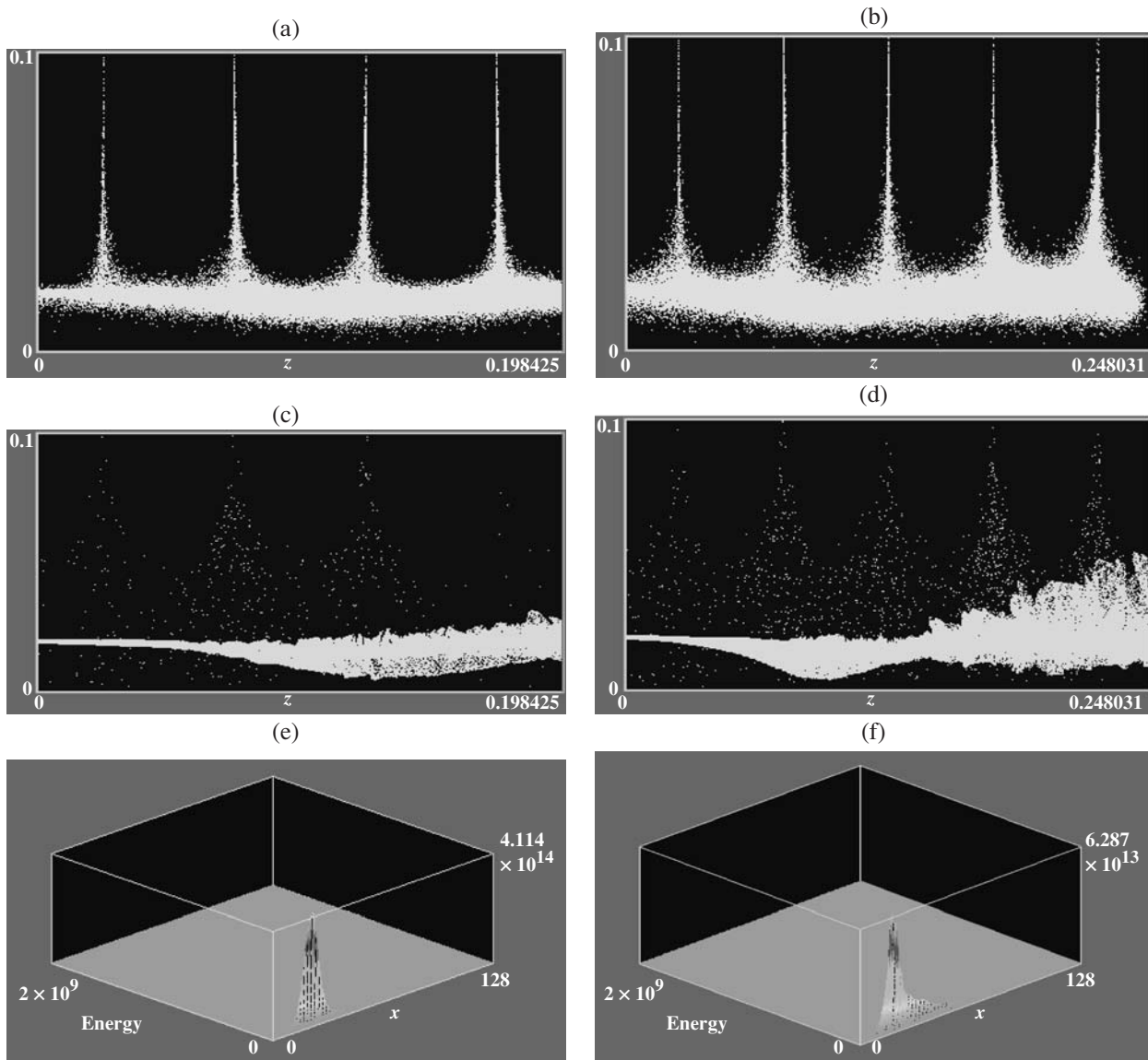


**Fig. 6.** Transport of a high-current NIB through (a, c, e) four and (b, d, f) five cusps: (a, b) electron and (c, d) ion distributions in the  $\{r, z\}$  plane and ion distribution functions  $F_i(\epsilon, r)$  ( $r = x \cdot r_L/128$ ) over energy and over the transverse coordinate at the right boundaries of the (e) fourth and (f) fifth cusps. The physical parameters of the problem are the same as in Fig. 3.

cases of the transport through one to five cusps shows that, as the number of cusps through which an NIB is transported is increased, the quality of  $F_i(\epsilon, r)$  decreases insignificantly.

Figure 7 illustrates the results of numerical simulations of the transport and acceleration of a high-current NIB through three cusps. Shown are the electron (Figs. 7a–7c) and ion (Figs. 7d–7f) distribution in the computation region as well as the ion distribution functions  $F_i(\epsilon, r)$  at the right boundary of the third (last) cusp (Figs. 7g–7i).

Figures 7a, 7d, and 7g refer to the case in which a high-current ion beam injected into the computation region at the velocity  $v_{i0} = 0.285c$  is accompanied by

an electron beam injected at the initial velocity  $v_{e0} = 0.8c$ , the accelerating field being zero. At the instant of injection, the current densities of the ion and electron beams are the same and conditions (2) and (3) are satisfied. As in the numerical cases illustrated in Figs. 3 and 6, some electrons of the neutralizing beam are lost in each cusp (Fig. 7a), so the ion beam becomes slightly unneutralized. From Figs. 7d and 7g we can see that, after the passage through the three cusps, the ion beam is slightly divergent and monoenergetic with a kinetic energy of 40.6 MeV. Figures 7b, 7e, and 7h illustrate the results of simulating the acceleration of this high-current NIB through three cusps. The physical parameters of the problem are the same as those in Figs. 7a, 7d,

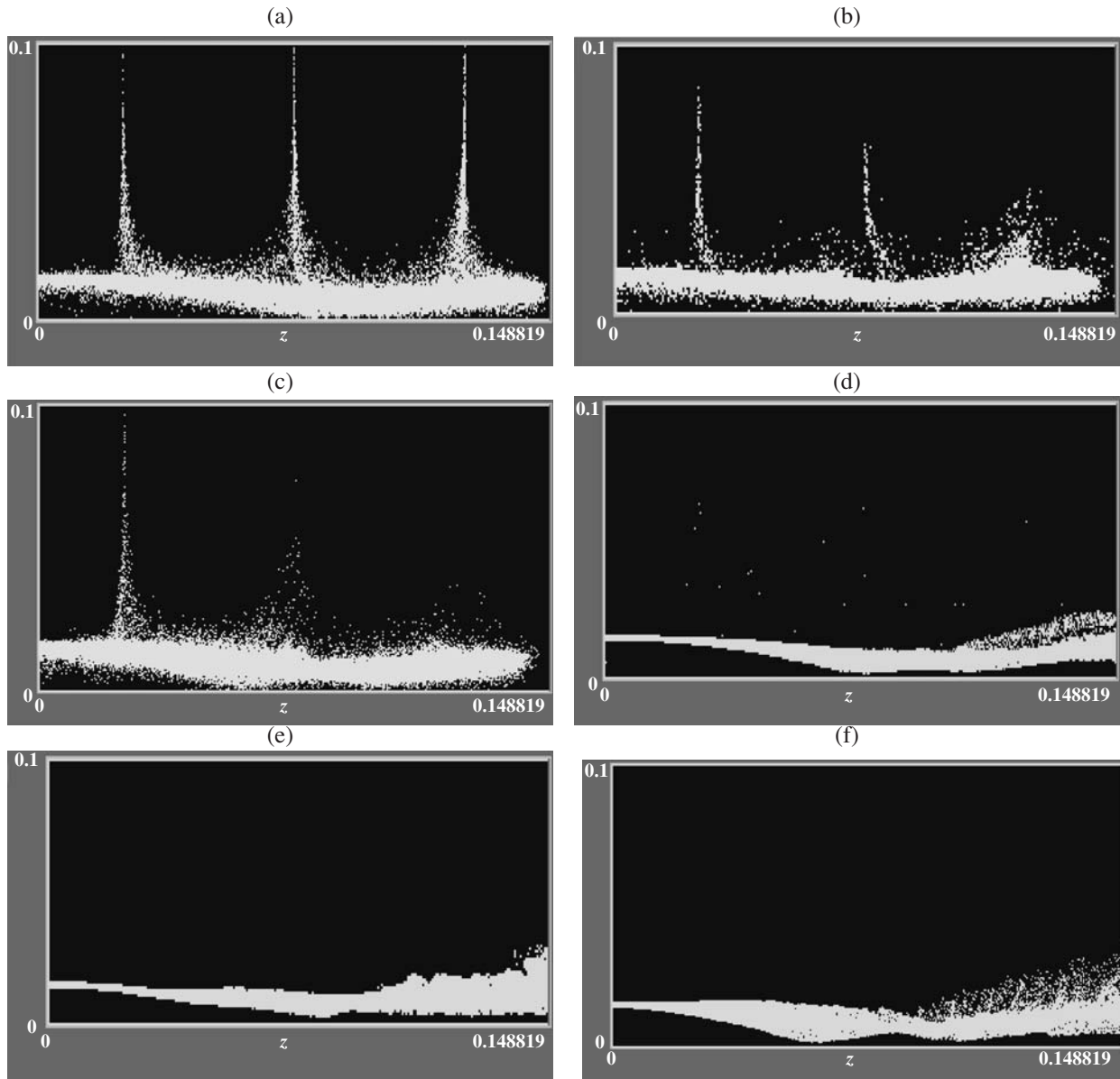


**Fig. 7.** (a, d, g) Transport and (b, e, h; c, f, i) acceleration of a high-current NIB through three cusps: (a–c) electron and (d–f) ion distributions in the  $\{r, z\}$  plane and (g–i) ion distribution function  $F_i(\epsilon, r)$  ( $r = x \cdot r_L/128$ ) at the right boundary of the third cusp. The parameters are  $H_0 = 47$  kG,  $v_{i0} = 0.285c$ ,  $n_{e0} = 7 \times 10^{19} \text{ m}^{-3}$ ,  $r_{\min} = 0.0142$  m, and  $r_{\max} = 0.0158$  m, the injection velocity of the electron beam and the accelerating field being (a, d, g)  $v_{e0} = 0.8c$  and  $E_z = 0$ , (b, e, h)  $v_{e0} = 0.8c$  and  $E_z = 460$  MV/m, and (c, f, i)  $v_{e0} = 0.99c$  and  $E_z = 460$  MV/m.

and 7g, except for the field  $E_z$  within the accelerating gaps, which is now 460 MV/m. From Fig. 7b we can see that, although the accelerating field, which decelerates the electrons, is strong, the neutralizing electron beam drifts in the self-consistent fields together with the ion beam, accompanying the latter through all the three cusps. In this case, as in the case without an accelerating electric field, some of the beam electrons are lost in each cusp and the energy required for the electrons to overcome the electric field accelerating the ions

is drawn from the kinetic energy of the ion beam—an effect that influences the quality of the ion distribution function at the right boundary of the third cusp (Fig. 7h). From Fig. 7h we can see that the ion energy distribution function at this boundary, although nonmonoenergetic, contains a large group of ions accelerated to an energy of 63.7 MeV. It should also be noted that, as is seen from Figs. 7e and 7h, the ion distribution function over the transverse coordinate does not degrade substantially. The results presented in Figs. 7c, 7f, and 7i

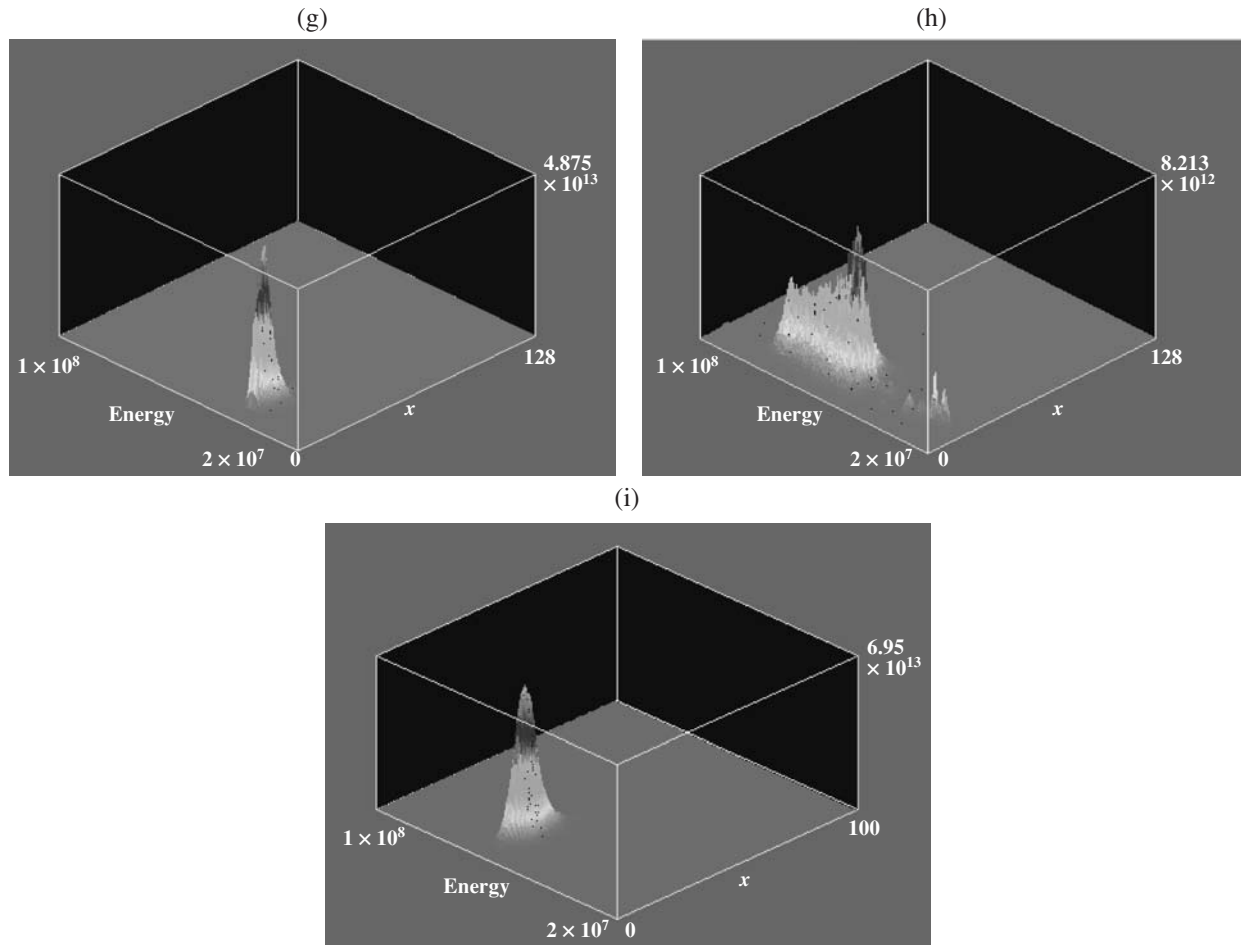


Fig. 7. (Contd.)

were calculated for a higher injection velocity of the electron beam,  $v_{e0} = 0.99c$ , the remaining parameters being the same as in Figs 7b, 7e, and 7h. From Fig. 7i we can see that the ion energy distribution function at the right boundary of the third cusp is essentially monoenergetic, with an energy of 63.7 MeV.

It has been shown above that, during the transport and acceleration of a high-current NIB, some electrons are lost in each of the cusps, so the ion beam becomes unneutralized. In addition, the electrons drifting in the self-consistent fields should overcome the electric field accelerating the ions. If the kinetic energy of the electrons is low, then they draw the required energy from the ion beam, with the result that the ion energy distribution function becomes wider. In order for the high-current NIB not to become unneutralized and the energy distribution function of the accelerated ions not to degrade substantially, it is necessary to inject an additional cold electron beam into each of the cusps. Figure 8 illustrates the results of simulating the acceleration of a high-current NIB through three cusps with the additional injection of a cold electron beam into

each cusp (see also Fig. 2). The parameters of the problem corresponding to Figs. 8a, 8c, and 8e are the same as those in Figs. 7b, 7e, and 7h, the only difference being that an additional electron beam, identical to the main (original) electron beam, is injected into each cusp. The parameters of the problem corresponding to Figs. 8b, 8d, and 8f are the same as those in Figs. 7c, 7f, and 7i, the only difference being the same: an additional electron beam, identical to the main electron beam, is injected into each cusp. From Figs. 8e and 8f we can see that the quality of the ion energy distribution function is far higher than that in the case without injection of additional electron beams: the accelerated ions are essentially monoenergetic, with an energy of 63.7 MeV. From Figs. 8e and 8f we can also see that the higher the energy of the neutralizing electron beams, the better the radial focusing of the accelerated ion beam.

#### 4. CONCLUSIONS

In the present paper, we have reported results of numerical particle simulations of the transport and

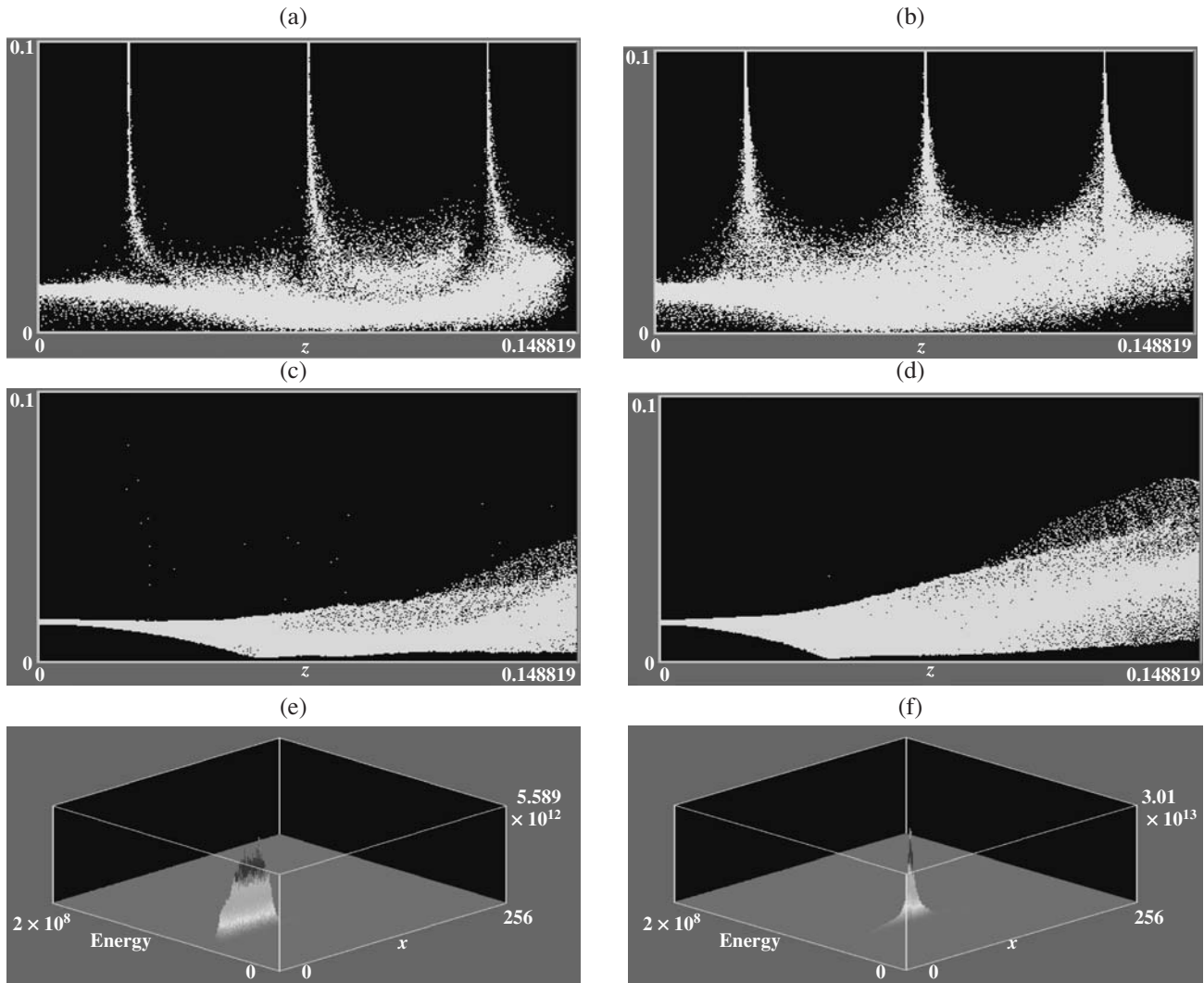


**Fig. 8.** Acceleration of a high-current NIB through three cusps with steady injection of an additional high-current electron beam: (a, b) electron and (c, d) ion distributions in the  $\{r, z\}$  plane and (e, f) ion distribution functions  $F_i(\epsilon, r)$  ( $r = x \cdot r_L/256$ ) over energy and over the transverse coordinate at the right boundary of the third cusp. The parameters are  $H_0 = 47$  kG,  $v_{i0} = 0.285c$ ,  $n_{e0} = 7 \times 10^{19} \text{ m}^{-3}$ ,  $r_{\min} = 0.0142$  m, and  $r_{\max} = 0.0158$  cm, the accelerating field and the injection velocity of the electron beam being  $E_z = 460$  MV/m and (a, c, e)  $v_{e0} = 0.8c$  and (b, d, f)  $v_{e0} = 0.99c$ .

acceleration of a tubular HCIB, accompanied by a neutralizing electron beam, through several magnetically insulated accelerating gaps. The simulations involve solving Maxwell's equations and relativistic equations of particle motion. We have demonstrated that a high-current NIB can be transported through one to five cusps. We have shown that, when conditions (2) and/or (3) fail to hold, the neutralizing electron beam is lost and a high-current ion beam cannot be transported. We have established that the quality of a high-current ion beam at the exit from the accelerator can be substantially improved by increasing the energy of the accompanying electron beam. We have also shown that, by injecting additional high-current electron beams into

the cusps, the accelerated ion beam can be made more monoenergetic and its divergence at the exit from the accelerator can be reduced.

## REFERENCES

1. *Inertial Confinement Fusion: Current State and Prospects for Power Engineering*, Ed. by B. Yu. Sharkov (Fizmatlit, Moscow, 2005) [in Russian].
2. O. V. Batishchev, V. I. Golota, V. I. Karas', et al., *Fiz. Plazmy* **19**, 611 (1993) [*Plasma Phys. Rep.* **19**, 313 (1993)].
3. B. Sharkov, D. Koshkarev, and M. Churasov, *Nucl. Instrum. Methods Phys. Res. A* **415**, 20 (1998).

4. R. O. Bangerter, Preprint No. LBL-33798 (Lawrence Berkeley Laboratory, Berkeley, CA, 1993).
5. A. Friedman, R. O. Bangerter, and W. B. Herrmannsfeld, Preprint No. UCRL-JC-117332 (Lawrence Livermore National Laboratory, Livermore, CA, 1994).
6. J. Barnard, R. Bangerter, A. Faltens, et al., Nucl. Instrum. Methods Phys. Res. A **415**, 218 (1998).
7. S. S. Yu, W. R. Meier, R. P. Abbott, et al., Preprint No. UCRL-JC-150169-REV-1 (Lawrence Livermore National Laboratory, Livermore, CA, 2002).
8. Yu. E. Kolyada, E. A. Kornilov, Ya. B. Fainberg, and V. A. Kiyashko, Pis'ma Zh. Tekh. Fiz. **2**, 916 (1976) [Sov. Tech. Phys. Lett. **2**, 359 (1976)].
9. V. A. Kiyashko, Yu. E. Kolyada, E. A. Kornilov, and Ya. B. Fainberg, Pis'ma Zh. Tekh. Fiz. **3**, 1257 (1977) [Sov. Tech. Phys. Lett. **3**, 519 (1977)].
10. V. A. Kiyashko, E. A. Kornilov, and V. A. Vinokurov, Vopr. At. Nauki Tekh., Ser. Tekh. Fiz. Eksp., No. 3, 21 (1987).
11. V. I. Karas', V. A. Kiyashko, E. A. Kornilov, and Ya. B. Fainberg, Nucl. Instrum. Methods Phys. Res. A **278**, 245 (1989).
12. V. I. Karas', E. A. Kornilov, and Ya. B. Fainberg, Vopr. At. Nauki Tekh., Ser. Plazm. Élektron. Nov. Metody Uskor., No. 1, 101 (1998).
13. A. I. Morozov and S. V. Lebedev, *Reviews of Plasma Physics*, Ed. by M. A. Leontovich (Atomizdat, Moscow, 1974; Consultants Bureau, New York, 1980), Vol. 8.
14. V. I. Karas', V. V. Mukhin, V. E. Novikov, and A. M. Naboka, Fiz. Plazmy **13**, 494 (1987) [Sov. J. Plasma Phys. **13**, 281 (1987)].
15. W. Peter and N. Rostoker, Phys. Fluids **25**, 730 (1982).
16. N. G. Belova, V. I. Karas', and Yu. S. Sigov, Fiz. Plazmy **16**, 209 (1990) [Sov. J. Plasma Phys. **16**, 115 (1990)].
17. N. G. Belova and V. I. Karas', Fiz. Plazmy **21**, 1065 (1995) [Plasma Phys. Rep. **21**, 1005 (1995)].
18. V. I. Karas' and N. G. Belova, Fiz. Plazmy **23**, 355 (1997) [Plasma Phys. Rep. **23**, 328 (1997)].
19. C. K. Birdsall, IEEE Trans. Plasma Sci. **19**, 65 (1991).
20. O. V. Manuilenko and K. M. Minaeva, Problems At. Sci. Technol., Ser. Plasma Electron. New Methods Accelerat., No. 5, 116 (2006).
21. O. V. Manuilenko, K. M. Minaeva, and V. I. Golota, Problems At. Sci. Technol., Ser. Plasma Phys., No. 6, 228 (2006).
22. J. K. Lee, N. Y. Babaeva, H. C. Kim, et al., IEEE Trans. Plasma Sci. **32**, 47 (2004).
23. J. K. Lee, O. V. Manuilenko, N. Y. Babaeva, et al., Plasma Sources Sci. Technol. **14**, 89 (2005).
24. Ch. K. Birdsall and A. B. Langdon, *Plasma Physics via Computer Simulation* (McGraw-Hill, New York, 1985; Énergoatomizdat, Moscow, 1989).
25. K. S. Yee, IEEE Trans. Antenna Propagat. **14**, 302 (1966).
26. A. B. Langdon, Comp. Phys. Comm. **70**, 447 (1992).
27. P. J. Mardahl and J. P. Verboncoeur, Comp. Phys. Comm. **106**, 219 (1997).
28. R. L. Morse and S. W. Nielson, Phys. Fluids **14**, 830 (1971).
29. J. Villasenor and O. Buneman, Comp. Phys. Comm. **69**, 306 (1992).
30. J. P. Verboncoeur, A. B. Langdon, and N. T. Gladd, Comp. Phys. Comm. **87**, 199 (1995).

*Translated by O.E. Khadin*

Copyright of Plasma Physics Reports is the property of Springer Science & Business Media B.V. and its content may not be copied or emailed to multiple sites or posted to a listserv without the copyright holder's express written permission. However, users may print, download, or email articles for individual use.